Heliyon

Received:
24 June 2018
Revised:
30 August 2018
Accepted:
3 September 2018

Cite as: Barbara Cerroni, Rosella Cicconi, Letizia Oddo, Manuel Scimeca, Rita Bonfiglio, Roberta Bernardini, Graziana Palmieri, Fabio Domenici, Elena Bonanno, Maurizio Mattei, Gaio Paradossi. *In vivo* biological fate of poly(vinylalcohol) microbubbles in mice. Heliyon 4 (2018) e00770. doi: 10.1016/j.heliyon.2018.e00770

In vivo biological fate of poly(vinylalcohol) microbubbles in mice

Barbara Cerroni [a,*], Rosella Cicconi [b], Letizia Oddo [a], Manuel Scimeca [c,d,e], Rita Bonfiglio [f], Roberta Bernardini [b], Graziana Palmieri [b,g], Fabio Domenici [a], Elena Bonanno [f], Maurizio Mattei [b,h], Gaio Paradossi [a]

[a] *Dipartimento di Scienze e Tecnologie Chimiche, Università degli Studi di Roma "Tor Vergata", via della Ricerca Scientifica 1, 00133 Rome, Italy*

[b] *Centro Servizi Interdipartimentale-Stazione per la Tecnologia Animale, Università degli Studi di Roma "Tor Vergata", via Montpellier 1, 00133 Rome, Italy*

[c] *Dipartimento di Biomedicina e Prevenzione, Università degli Studi di Roma "Tor Vergata", via Montpellier 1, 00133 Rome, Italy*

[d] *Università San Raffaele, via di Val Cannuta 247, 00166, Rome, Italy*

[e] *OrchideaLAB S.r.l., via del Grecale 6, 00067 Morlupo, Rome, Italy*[1]

[f] *Dipartimento di Medicina Sperimentale e Chirurgia, Università degli Studi di Roma "Tor Vergata", via Montpellier 1, Rome 00133, Italy*

[g] *Plaisant Srl, Via Castel Romano 100, 00128 Rome, Italy*

[h] *Dipartimento di Biologia, Università degli Studi di Roma "Tor Vergata", via della Ricerca Scientifica 1, 00133 Rome, Italy*

[*] Corresponding author.

E-mail address: barbara.cerroni@uniroma2.it (B. Cerroni).

[1] www.orchidealab.it.

Abstract

Microbubbles (MBs) are used in clinical practice as vascular ultrasound contrast agents, and are gaining popularity as a platform supporting multimodal imaging and targeted therapy, facilitating drug delivery under ultrasound exposure. Here, we report on the *in vivo* biological impact of newly discovered MBs with promising features as a multimodal theranostic device. The shell of the air-filled MBs is made of the poly(vinyl alcohol) (PVA), a well-established, FDA-approved polymer. Nevertheless, as size, shape and dispersity can significantly impact the

https://doi.org/10.1016/j.heliyon.2018.e00770

biological response of particulate systems, studying their fate after administration is crucial. The safety and the biodistribution of PVA MBs were analysed *in vivo* and *ex vivo* by coupling a near infrared (NIR) fluorophore on their shell: MBs accumulated mainly in liver and spleen at 24 hours post-injection with their clearance from the spleen 7 days post-dosing. A possible way of elimination was identified in macrophages ability to engulf MBs both *in vitro* and *in vivo*. One month post-dosing, transmission electron microscopy (TEM) highlighted the lack of relevant defects and the elimination of PVA MBs by Kupffer cells. This study is the first successful attempt to fill the lack of knowledge necessary to bring PVA MBs one step closer to their possible clinical use.

Keywords: Biochemistry, Bioengineering, Cell biology, Medical imaging

1. Introduction

Ultrasound contrast agents (UCAs) in the form of microbubbles (MBs) are used clinically to increase the sensitivity and specificity of diagnostic ultrasonography. MBs are gas-filled voids with a diameter ranging from 1 to 8 μm, stabilised by an elastic shell (2−500 nm) composed of lipids, polymers or both (i.e. hybrid MBs) [1, 2, 3]. Owing to their ability to resonate when exposed to an ultrasound (US) field, they improve the scattering of the US wave thereby acting as "echo-enhancers". The reflection of a strong US signal depends on several parameters such as bubble size, concentration, gas pressure, and surface tension [4, 5].

Over the years, the biomedical research has addressed to the implementation of UCAs in order to upgrade diagnostic agents turning them into theranostic devices. In this perspective, MBs made of poly(vinyl alcohol) (PVA) have generated substantial interest for their promising potentialities in terms of improved stability and facile surface functionalisation for multimodal and targeting purposes. Therefore, understanding the fate of PVA MBs once injected into the blood circulation is of crucial importance in order to bring PVA MBs one step forward to clinical use.

PVA MBs are US-active [6, 7], 3-μm sized particles made of a highly hydrated polymer shell of 200 nm thickness [8]. Their formation occurs during the foaming of oxidised telechelic PVA in an aqueous medium. At the water/air interface the air contained in the foam remains entrapped in the crosslinked PVA network forming the gas core of the MBs [9].

The advantages of the PVA MBs lie in the shell as they show an excellent stability and versatility when compared to lipid shelled MBs. *In vitro* the cross-linked shell of PVA MBs has a remarkable shelf life of several months [9]. Marketed lipid Sonovue MBs show an elimination half-life in the bloodstream of approximately 6 minutes and often more than one injection is required during an ultrasound investigation

https://doi.org/10.1016/j.heliyon.2018.e00770

[10]. An increased stability is desirable especially in view of next generation UCAs for targeted molecular imaging. One of the problems of the targeting is that the number of adhering MBs is small in comparison to those in circulation, which generates a high background signal that can impair the detection of the target [11]. Waiting for the clearance of free MBs by the reticuloendothelial system is a possibility to overcome this problem but to this aim prolonged stability of microbubbles is required [12, 13]. On the other hand an excess of stability is not desirable as the key issues for injectable devices are the biodegradation and the bioelimination. Studies on the enzymatic degradation of PVA by different bacterial strains have been reported [14, 15, 16] while in animals the biodegradability and/or elimination of PVA is still under debate, despite the encouraging results of Kaneo et al. [17] concerning intravenously (IV) injected PVA.

The chemical versatility of PVA MBs depends on the hydroxyl and aldehyde moieties (masked at physiological pH as hemiacetals) [9], which can be exploited for the tethering of active molecules thereby promoting targeted drug delivery [18, 19, 20, 21]. Moreover, the opportunity to conjugate dyes and magnetic nanoparticles on the shell fulfils the requirements of the diagnostic research which yearn for the availability of one injectable device that can permit multimodal imaging: US + Fluorescence + Magnetic Resonance Imaging (MRI). We have already demonstrated that superparamagnetic iron oxide nanoparticles successfully implement the modalities of the PVA MBs, enabling the activity of the MBs for MRI [22]. Among fluorescent probes, Near Infrared (NIR) fluorophores are gaining attention due to the following advantages: (i) tissues irradiated with NIR wavelengths present low absorption and low scattering, allowing images to be acquired with minimal tissue autofluorescence; (ii) NIR wavelengths can penetrate deeper into the skin going beyond the limit of 1−2 mm depth of the fluorescence imaging in the visible field [23, 24]. The so-modified PVA MBs become a platform which combines the dual function of the real-time multimodal imaging and the *in situ* treatment of diseases such as tumours, decreasing the side effects linked to systemic tumour chemotherapies [25].

Despite the lack of information regarding the *in vivo* safety of PVA MBs, a lot is known about the polymer. It is an FDA-approved biocompatible, non-toxic, inert synthetic polymer which already has several *in vivo* applications as a material for contact lenses, eye wetting drops and in implantable devices such as catheters, vascular embolic agents, tissue adhesion barriers and for cartilage replacements and nerve guide [26]. Moreover, it is often used alone or as part of copolymers for biomedical applications [27, 28, 29, 30, 31, 32]. Other synthetic polymers such as poly(lactide-co-glycolide) (PLGA) [33], poly(DL-lactide) (PLA), polyalkylcyanoacrylate, and polycaprolactone (PCL) polymers [34] are commonly used as starting material for the synthesis of particles in biomedicine. The attention towards the use of synthetic polymers as biomaterials is justified by the fact that they are not affected by limitations in terms of synthesis and processing, as can be the case for

https://doi.org/10.1016/j.heliyon.2018.e00770

natural ones. Moreover, they give the possibility to fabricate new systems with controlled and tailored detailed structures. *In vivo* studies on PVA MBs presented in this manuscript were guided by *in vitro* tests that showed good biocompatibility in different cell lines [35, 36].

The aim of this paper is to understand the biological impact of the injectable PVA MBs *in vivo*, studying the biodistribution/bioelimination in a mouse model; these issues are pivotal and not predictable as they depend on several variables such as the route of injection, the size, shape and dosing of the administered system, and at last, but not least, the specific PVA texture (i.e., type and amount of chemical crosslinks as well as of physical entanglements networking PVA chains building up the shell structure).

The study of the PVA MBs fate was followed from short to long term in the entire animal mouse, until one month post-intravenous injection. The labelling of the PVA MBs with the NIR DyLight755 (DyL) fluorophore and the combination of different imaging techniques have allowed the more detailed assessment of their safety bringing them one step closer to their possible clinical use.

2. Materials and methods

2.1. Synthesis of DyLight755-MBs

PVA MBs were synthesised as reported elsewhere [9]. Briefly, 4 g of PVA (number-average molecular weight of 30,000 ± 5,000 g/mol and weight-average molecular weight of 70,000 ± 10,000 g/mol, Sigma-Aldrich, Milan, Italy) were dissolved in 200 mL of Milli-Q (18.2 MΩ cm) water at 80 °C under constant stirring. After complete PVA dissolution, the oxidation reaction was carried out by the addition of 0.380 g of $NaIO_4$ (Sigma-Aldrich, Milan, Italy) at 80 °C for 1 hour under stirring. Then, the solution was cooled to room temperature, and vigorously stirred for 2 hours at 8,000 rpm by an Ultra-Turrax T-25 (IKA®, Germany), equipped with a Teflon-coated tip. Floating MBs were separated from solid debris in separatory funnels and several washings were carried out until no debris were observed. The concentration of the obtained MBs was determined by using a cell counting chamber slide for microscopy (Neubauer Chamber) and it was expressed as number of MBs/mL.

MBs were fluorescently-labelled using the DyLight755 N-hydroxysuccinimide (NHS) ester (ThermoFisher Scientific, Milan, Italy). The dye was dissolved in dimethylformamide (10 mg/mL, Sigma-Aldrich, Milan, Italy) and added to around 4×10^9 MBs suspended in 1.25 mL of 0.1 M sodium carbonate at pH 8.4 for 1 hour. Excess unbound dye was removed by several washings with Milli-Q water and the labelled MBs were resuspended in saline (NaCl 0.9%). The synthesised DyLight755-labelled PVA MBs are referred in the text as DyL-MBs. The DyL-MBs

https://doi.org/10.1016/j.heliyon.2018.e00770

were observed by confocal laser scanning microscopy (CLSM, Nikon Eclipse Ti-E C1, Japan).

2.2. Animal model

Six to eight-week-old female CD1 mice (Charles River, Lecco, Italy) were used. All experiments were carried out at the Centro Servizi Interdipartimentale-Stazione per la Tecnologia Animale, Università degli Studi di Roma "Tor Vergata", approved by the Animal-Welfare body and carried out in accordance with Italian and European rules. All the animal experiments were ethically approved and authorised by the General Director of the Ministry of Health, Legislative Decree no. 26/2014; European Directive 2010/63/UE; Authorisation number issued by Ministry of Health 430/2017-PR. Animals were housed under standard conditions: light/dark cycles (12/12 h), ambient temperature 20 ± 2 °C, 55% relative air humidity and food (4RF18, Mucedola, Milan, Italy) and water *ad libitum*. A veterinary surgeon, responsible for the welfare of laboratory animals, was present during all sets of experiments. Animal care was under the responsibility of trained personnel.

For all experiments a volume of 100 μL of MB suspension (10^8 MBs/mL), both labelled and unlabelled MBs, or of free DyL (2 mg/mL), was administered to mice using three mice *per* group. For biodistribution and elimination studies mice were injected IV via the retro-orbital plexus under general anaesthesia, whereas for the study concerning the macrophage interaction with MBs, mice were injected intraperitoneally. When necessary, mice were anaesthetised with an intraperitoneal injection of ketamine (Ketaset, 100 mL/kg, MSD Animal Health, Milan, Italy) and xylazine (Rompun, 15 mL/kg, Bayer, Milan, Italy).

Blood collection was performed by retro-orbital sinus puncture under general anaesthesia.

After the injection, gross visual observations were made daily for general condition (appearance, demeanour, appetite, hydration, body weight and food consumption).

Euthanasia of anaesthetised mice employed throughout the different experimental procedures was carried out by cervical dislocation as recommended by Legislative Decree no. 26/2014, annex IV.

2.3. Haematology and clinical biochemistry

For determination of haematological parameters, 20 μL of whole blood were collected in K2 EDTA microtainers (Becton Dickinson, Milan, Italy) and the samples were analysed using the commercially available automated cell counter "Drew3" (BPC BioSed, Rome, Italy). Haematological parameters [red blood cell (RBC) counts, haemoglobin (HGB), haematocrit (HCT), white blood cell (WBC)

https://doi.org/10.1016/j.heliyon.2018.e00770

total and relative differential counts as lymphocytes (LYMF), mid-range cells (MID), granulocytes (GRAN), mean corpuscular haemoglobin (MCH), mean corpuscular volume (MCV), mean corpuscular haemoglobin concentration (MCHC) and platelet counts (PLT), red cell distribution width (RDW), mean platelet volume (MPV)] were analysed.

For determination of clinical chemistry parameters, blood samples were collected in SST microtainers (Serum Separator Tube; Becton Dickinson, Milan, Italy) and centrifuged in a microcentrifuge (5415R model; Eppendorf, Italy) at 13,000 rpm for 7 min to separate the serum. Aspartate aminotransferase (AST), alanine aminotransferase (ALT), blood urea nitrogen (BUN) and creatinine (CRE) were measured using the automatic analyser Keylab (BPC BioSed. Rome, Italy).

2.4. In vivo and ex vivo fluorescence imaging

A Kodak FX image station 4000 mm was used for *in vivo* and *ex vivo* image acquisition of mice injected with a volume of 100 μL of DyL-MB suspension (10^8 MBs/mL) or the free dye (2 mg/mL).

The loading of the dye *per* PVA MB was estimated by comparing the signal emission of different amount of free dye with that emitted by a known number of labelled PVA-MBs.

Before treatment with MBs, all mice were anaesthetised. At different time points, they were positioned ventrally or dorsally on the stage of the image station and non-invasively imaged by combining X-rays and fluorescence in the NIR region (excitation filter: 720 $\pm$ 10 nm; emission filter: 790 $\pm$ 20 nm).

Mice were sacrificed at 100 minutes, 24 hours and 7 days post-injection. Heart, thymus, liver, spleen, lungs, kidneys and pancreas were collected for the *ex vivo* analysis. The fluorescence signals were registered and overlaid with the X-ray image. Regions of interest (ROIs) were drawn over the signals, and the sum of the fluorescence intensity of each ROI was measured and divided by the area of all the organs. Fluorescence image quantification was carried out by using the freeware ImageJ package.

2.5. Macrophage interaction with MBs

In vitro: murine monocyte/macrophage RAW 264.7 (purchased from Istituto Zooprofilattico della Lombardia e dell'Emilia Romagna, Italy) were maintained in culture at 37 °C in a 5% CO_2 atmosphere. Cells were cultured in Dulbecco's modified eagle medium (DMEM) with low glucose (1,000 mg/L) supplemented with 10,000 U/mL penicillin-streptomycin, 1% L-glutamine and 10% v/v of heat-inactivated foetal bovine serum (Sigma-Aldrich, Milan, Italy).

https://doi.org/10.1016/j.heliyon.2018.e00770

RAW 264.7 cells (~500,000 cells) were treated with PVA MBs (10^7 MBs) in a SmartSlide™-6 Micro-Incubator (WaferGen Biosystems, Fremont, CA) to maintain controlled cell conditions of temperature and CO_2 under the light microscope (Nikon Inverted Microscope Eclipse Ti-E, Japan). After cell seeding, MBs were added and a time-lapse experiment (time frame: 30 seconds) was carried out.

In vivo: PVA MBs (100 μL of 10^8 MBs/mL) were injected intraperitoneally into CD1 mice. After 1.5 hours, mice were sacrificed; phosphate buffered saline (PBS, 5 mL) at 4 °C was injected into the peritoneum followed by gentle massage to promote the detachment of macrophages. A small incision was made in the ventral abdomen to withdraw macrophages suspended in PBS. After one washing in PBS, the sample was fixed and stored in 10% formalin and observed by microscopy (Nikon Inverted Microscope Eclipse Ti-E optical microscopy and scanning electron microscopy).

2.6. Scanning electron microscopy (SEM) analysis

The sample described above was post-fixed in 2% osmium tetroxide. After washing with 0.1 M PBS, the sample was dehydrated by a series of incubations in 30%, 50% and 70% (v/v) ethanol. Dehydration was continued by incubation steps in 95% (v/v) ethanol, absolute ethanol and acetone. Critical-point drying (Agar Scientific, Elektron Technology, UK) with supercritical CO_2 was then performed to prevent cell deformation. Surfaces of the scaffolds were coated with gold and scanned using SEM LEO 1450VP (Carl Zeiss Meditec, Germany) [37].

2.7. Transmission electron microscopy(TEM) and energy dispersive x-ray (EDX) microanalysis

After injection with unlabelled PVA MBs, mice were sacrificed at 10 minutes and 30 days post-injection after collection of blood. Organs (liver, lungs, kidney) were collected and fixed at 4 °C in 10% buffered formalin for 24 hours and post-fixed in 2% osmium tetroxide. Tissues were embedded in paraffin and sectioned. After washing with 0.1 M PBS, each sample was dehydrated by a series of incubations in 30%, 50%, 70%, 95% ethanol. Dehydration was continued by incubations in absolute ethanol and propylene oxide. For ultrastructural analysis, the sample was then embedded in Epon resin [38] (Agar Scientific, Elektron Technology, UK). After inclusion, the tissue was cut and stained with heavy metals solutions (uranium acetate and lead citrate) as described by Reynolds [39]. All samples were examined by a Hitachi H-7100 FA transmission electron microscope (Hitachi, Schaumburg, IL, USA). For EDX microanalysis, unstained ultra-thin sections of approximately 100 nm-thick were mounted on copper grids for microanalysis. EDX spectra of microcalcifications were acquired with a Hitachi 7100FA transmission electron microscope (Hitachi, Schaumburg, IL, USA) and an EDX detector (Thermo Scientific,

https://doi.org/10.1016/j.heliyon.2018.e00770

Waltham, MA, USA) at an acceleration voltage of 75 keV and magnification of 12,000. Spectra were semi-quantitatively analysed by the Noram System Six software (Thermo Scientific, Waltham, MA, USA) using the standard-less Cliff-Lorimer k-factor method [40, 41]. The EDX microanalysis apparatus was calibrated using an x-ray microanalysis standard (Micro-Analysis Consultants, UK).

2.8. Statistical analysis

All results shown represent the means ± standard error of the mean (*SEM*) from triplicate experiments performed in a parallel manner. Statistical analyses were performed using a paired t-test. All comparisons were made relative to untreated controls and significance of difference is indicated as $*p < 0.05$.

3. Results

The fate of PVA MBs IV injected into mice was analysed over the time. MBs were labelled with the DyLight755, a fluorophore emitting at 776 nm, coupling the NHS ester of the dye with the hydroxyl groups of the PVA MB surface (Fig. 1A). The successful labelling of the PVA MBs was monitored by CLSM (Fig. 1B) and a quantitative estimation of 10^{10} DyL molecules *per* MB was estimated by comparing the emitted signal of the free dye with the labelled MBs, as registered by the Kodak FX image station 4000 (Fig. 1C).

The biodistribution of the DyL-MBs in mice was assessed and compared to the free NIR dye, DyL (Fig. 2). The fluorescent pattern was tracked every 10 minutes for the first 60 minutes, then the permanence of the signal was evaluated for longer timeframes, i.e. 24 hours and 7 days, to identify possible elimination processes. The pharmacokinetics of the free dye alone (Fig. 2b) was quicker than that one of the dye conjugated to MBs (Fig. 2a). Moreover the free dye accumulated only in the bladder, indicating its excretion was mainly via urine. These two evidences, taken together, allow to discriminate the fluorescence contribution due to a possible detachment of the dye from that one coming from the MBs. In contrast to the free dye, when mice were IV injected with DyL-MBs most of the fluorescent signal was detected in the mid-abdominal region. Starting from the first observation (20 minutes) the signal increased over the time, indicating the progressive and massive accumulation of DyL-MBs in the liver (Fig. 2a), whereas it was necessary to wait 40 minutes to have a slight fluorescent spot in the bladder.

As expected, using excitation wavelengths in the NIR window, autofluorescence was not detected in mice treated with saline (Fig. 2c) [42].

The *ex vivo* analysis permitted more precise localisation of fluorescence signal and its quantitative estimation at single organ level. The measurements were carried out

https://doi.org/10.1016/j.heliyon.2018.e00770

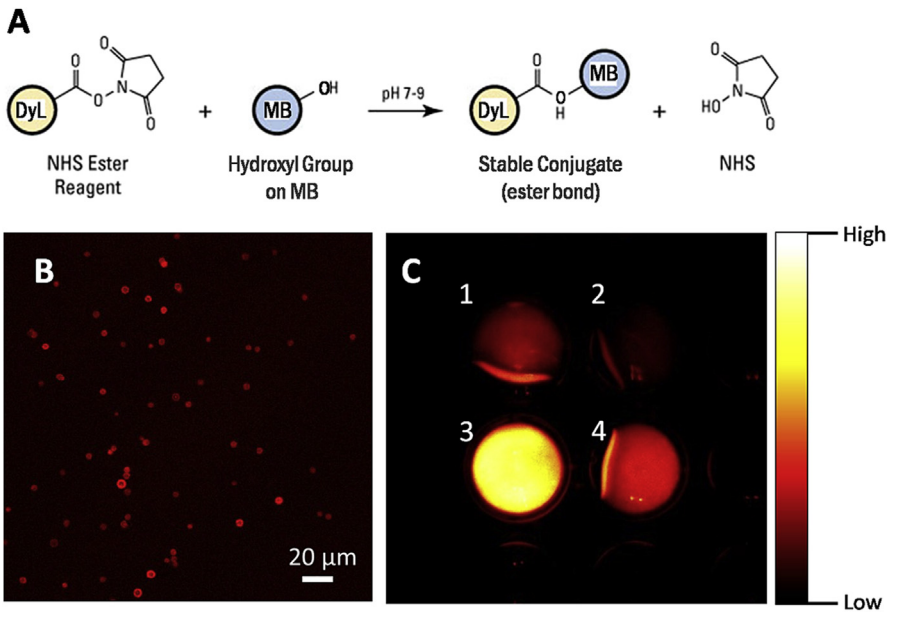

Fig. 1. Conjugation of the dye DyL on PVA MBs. (A) Chemistry of the conjugation of DyL on the hydroxyl groups of the PVA MBs through NHS ester reaction mechanism; (B) CLSM micrograph of labelled NIR MBs; (C) comparison between the fluorescence at 790 nm of free DyL, (C1) 0.1 mg/mL and (C2) 0.05 mg/mL, with respect to DyL-MBs number density (C3) 1.7×10^8 MBs/mL and (C4) 5.6×10^6 MBs/mL. The similarity in the fluorescence between C1 and C3 was used for the estimation of the extent of labelling. On the right side, a colour scale of the fluorescence intensity is reported for reference.

at 100 minutes, 24 hours and 7 days post-injection and they resulted in an increased detection in the number of the organs involved in the accumulation of the samples with respect to the *in vivo* evaluation (Fig. 3). An intense fluorescence signal was detected at 100 minutes post-injection in the heart, kidneys, lungs, spleen and liver of the mice treated with DyL-MBs and in the kidneys and spleen of the mice injected with the free dye DyL. At later time points a decrease in the fluorescence signal indicated a progressive clearance of the samples that still remained in the reticuloendothelial system organs, i.e. the spleen and the liver (Fig. 3).

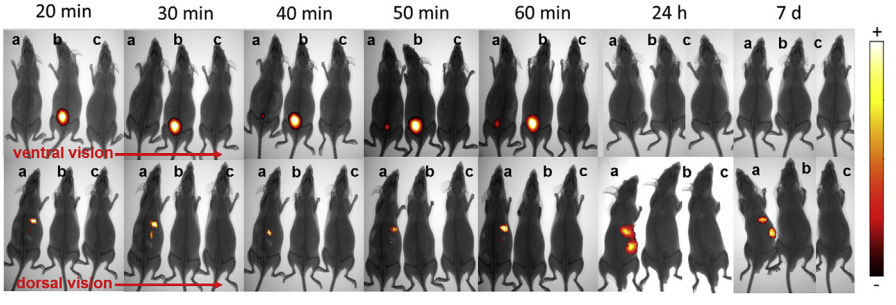

Fig. 2. Biodistribution of labelled MBs in CD1 mice. Biodistribution of (a) DyL-MBs, (b) DyL, and (c) saline in CD1 mouse observed at different times from injection. Each image is an overlay of the X-ray and fluorescence image. On the right side, a colour scale of the fluorescence intensity is reported.

https://doi.org/10.1016/j.heliyon.2018.e00770

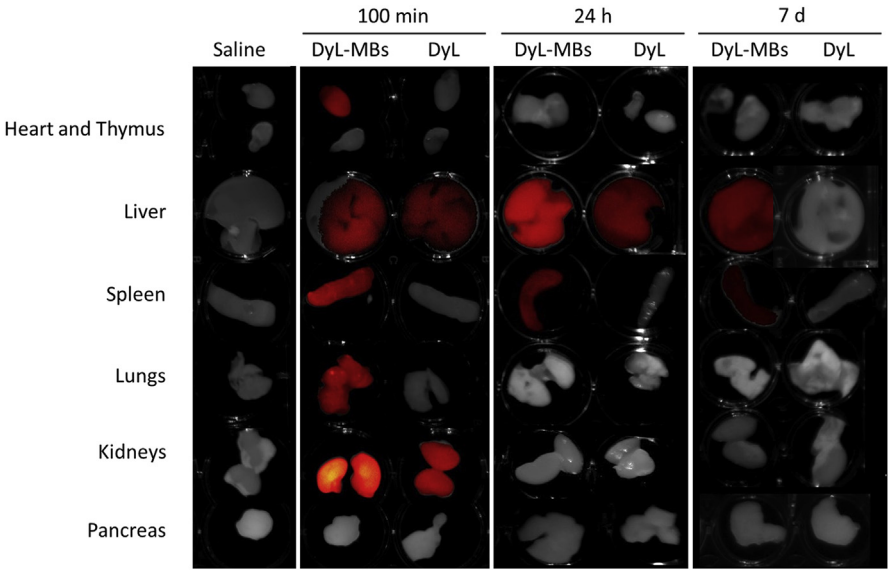

Fig. 3. Biodistribution of labelled MBs in organs. Ex vivo NIR imaging of organs isolated from mice treated either with saline, DyL-MBs or free DyL. Mice were euthanised and organs were kept at 100 minutes (min), 24 hours (h) or7 days (d) from the injection. Images are overlays of optical and fluorescence acquisition modes.

In particular, only the DyL-MBs but not the free dye DyL distributed in the spleen, anyway their net fluorescence intensity dropped over the time reaching values around five-fold lower than the initial ones (Fig. 4A). The liver was able to completely eliminate the free DyL in the time frame from 24 hours to 7 days after administration, while a net fluorescence increase of the DyL-MBs was observed in the liver 24 hours post-administration. After 7 days the fluorescence intensity decreased although it was still detectable (Fig. 4B).

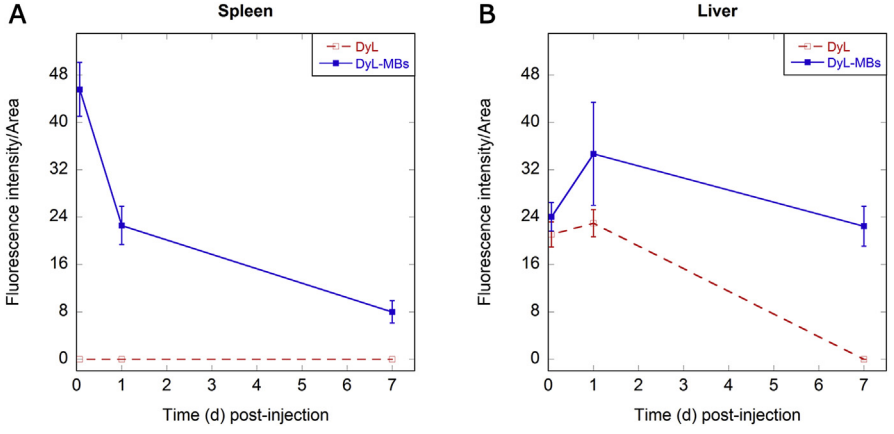

Fig. 4. Quantitative analysis of MB biodistribution in organs. Net fluorescence intensity normalised for organ area of the DyL (red line) and DyL-MBs (blue line) in mice (A) spleen and (B) liver. Error bars are the standard deviation observed in three independent experiments. First points report the Fluorescence/Area at 100 min. Time 0 refers to the time of injection.

https://doi.org/10.1016/j.heliyon.2018.e00770

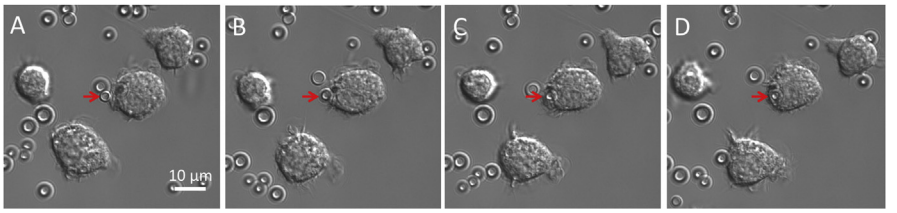

Fig. 5. In vitro phagocytosis of MBs. Optical micrograph of RAW 264.7 monocytes/macrophages incubated with PVA MBs. The red arrow highlights the phagocytosis process of the PVA MB during time (A) 0 minutes, (B) 1 minute, (C) 2 minutes, (D) 3 minutes.

The persistence of PVA MBs in the reticuloendothelial system organs suggests a possible involvement of the macrophages. The ability of macrophages to recognise and phagocytose PVA MBs was investigated both *in vitro* and *in vivo*. The *in vitro* study was carried out by incubating murine monocyte/macrophages RAW264.7 with MBs following the phagocytosis events by time-lapse experiment (Fig. 5), sustaining previous studies [43].

For the *in vivo* study, MBs were injected intraperitoneally into mice. SEM analysis of the isolated resident peritoneal macrophages showed clearly the cell plasma membrane approaching the MB surface suggesting an initial step of the internalisation process (Fig. 6, only part of the macrophage is highlighted).

The observation of MBs in the liver after 7 days from administration prompted us to extend the study to one month. The long-term experiment was justified by

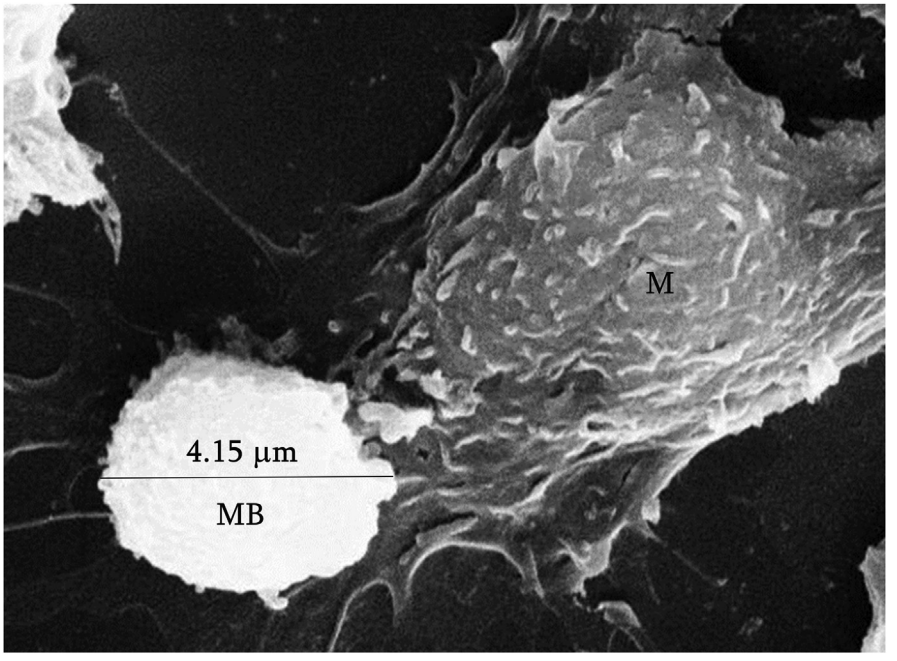

Fig. 6. In vivo adhesion of MBs to macrophages. SEM micrograph of a detail of a murine peritoneal macrophage (M) approaching a PVA MB (diameter of the MB is reported).

https://doi.org/10.1016/j.heliyon.2018.e00770

considering the robustness of the crosslinked polymer shell as compared to the labile lipid-based MBs. In this case the fluorescent imaging was not feasible due to hydrolytic degradation of the ester bonds linking the dye molecules to the MBs resulting in detachment of the dye from the MB shell and the occurrence of artefacts. On the other hand, TEM and SEM techniques can provide clearer results as MBs are directly observed in mouse tissue sections and, at the same time, the ultrastructural analysis of tissues gives information on the status of the single organs.

Over the course of the experiment, the general health condition of the mice was monitored in terms of changes in gait, posture and behaviour, and during this period, the mice appeared healthy with no differences in growth compared to control animals (Fig. 7A). At the end of the observations, mice were sacrificed and the organs of PVA MB-injected mice were weighed and compared with the weight of saline-injected ones, with no significant differences found (Fig. 7B). Haematology (Table 1) and biochemistry parameters (data not shown) confirmed the absence of clinically relevant alterations. However, the possible small variations in the number of blood white cells can be justified by the sensitivity of this parameter to the bacterial infections and housing conditions.

The ultrastructural analysis of lungs and kidneys confirmed the good biocompatibility of the MBs: after 10 minutes and 1 month post-injection no significant tissue alterations were identified.

In particular, as far as kidneys were concerned, after 10 minutes only limited ultrastructural alterations were observed in the glomerular areas (Fig. 8A) with a complete recovery after one month (Fig. 8B).

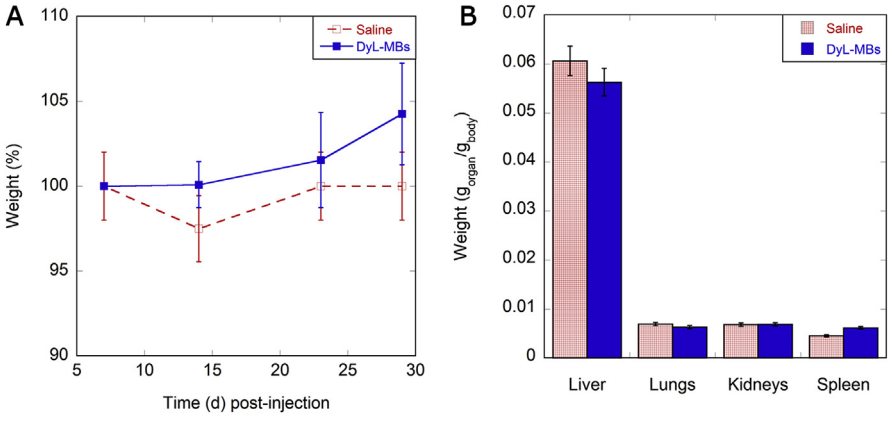

Fig. 7. General observations of the status of the injected mice. (A) Time course of mouse growth (d: days): increase in mouse weight at varying days after the injection of saline (dashed red line) and DyL-MBs (solid blue line). (B) Organ weights of saline (patterned red bars) and DyL-MBs (coloured blue bars) injected mice at 30 days after the administration. Organs weights are normalised with respect to the body weight of the animals.

https://doi.org/10.1016/j.heliyon.2018.e00770

Table 1. Effect of PVA MBs in mice at different times post-injection: complete blood count (CBC). To be considered that values with an asterisk are within the reference range although significantly differ from the control ($p < 0.05$).

CBC	Reference values	Control Mean ± SD	10 min Mean ± SD	100 min Mean ± SD	1 day Mean ± SD	7 days Mean ± SD	30 days Mean ± SD
WBC (10^3/mm^3)	5.0–12.0	8.5 ± 4.0	10.7 ± 3.6	6.7 ± 1.1	8.3 ± 2.4	11.2 ± 0.3*	9.8 ± 4.6
LYMF (%)	65.0–80.0	64.9 ± 8.8	74.0 ± 12.2	56.8 ± 10.2	69.6 ± 4.8	76.7 ± 2.4	73.9 ± 11.7
MID (%)	0.0–10.0	16.8 ± 10.1	9.4 ± 2.8	23.9 ± 8.1	5.2 ± 0.1	6.2 ± 0.8	7.0 ± 2.4
GRAN (%)	10.0–30.0	18.3 ± 3.1	16.5 ± 15.0	19.3 ± 4.5	25.2 ± 4.9	17.1 ± 2.1	19.2 ± 14.1
LYMF (10^3/mm^3)	4.0–10.0	5.6 ± 1.6	7.7 ± 1.8	4.0 ± 1.0	5.7 ± 1.3	8.6 ± 0.2*	7.6 ± 4.6
MID (10^3/mm^3)	0.0–2.0	1.3 ± 0.7	1.0 ± 0.3	1.5 ± 0.4	0.4 ± 0.2	0.7 ± 0.1	0.8 ± 0.6
GRAN (10^3/mm^3)	0.5–6.0	1.6 ± 0.4	2.1 ± 2.3	1.3 ± 0.5	2.2 ± 1.1	1.9 ± 0.3	1.4 ± 0.7
RBC (10^6/mm^3)	9.0–13.0	9.81 ± 0.54	9.49 ± 0.24	9.79 ± 0.86	9.32 ± 0.71	9.19 ± 0.33	9.1 ± 0.6
HGB (g/dL)	10.0–19.0	16.5 ± 0.7	16.8 ± 0.7	16.1 ± 0.5	16.3 ± 0.4	16.0 ± 1.0	14.5 ± 1.6
HCT (%)	40.0–55.0	44.3 ± 1.7	45.9 ± 2.0	44.6 ± 0.5	43.2 ± 0.6	42.3 ± 2.4	42.4 ± 2.2
MCV (μm^3)	39.0–49.0	45.2 ± 1.2	48.4 ± 3.4	45.8 ± 3.7	46.6 ± 4.3	46.0 ± 2.6	46.5 ± 2.5
MCH (pg)	13.0–20.0	16.8 ± 0.3	17.7 ± 1.1	16.5 ± 1.3	17.6 ± 1.8	17.5 ± 0.9	15.9 ± 1.2
MCHC (g/dL)	30.0–39.0	37.2 ± 0.9	36.6 ± 0.7	36.0 ± 0.8	37.7 ± 0.6	37.9 ± 0.8	34.1 ± 2.0
RDW (%)	0.0–99.9	16.2 ± 1.9	17.8 ± 0.2	17.9 ± 3.1	16.3 ± 0.9	16.4 ± 0.6	16.8 ± 1.2
PLT (10^3/mm^3)	600–1400	1077 ± 135	1059 ± 180.6	1423 ± 52*	1230 ± 194	1132 ± 139	1072.8 ± 638.4
MPV (μm^3)	4.0–7.0	5.2 ± 0.2	5.3 ± 0.2	5.2 ± 0.3	5.1 ± 0.1	5.2 ± 0.3	5.9 ± 0.8

https://doi.org/10.1016/j.heliyon.2018.e00770

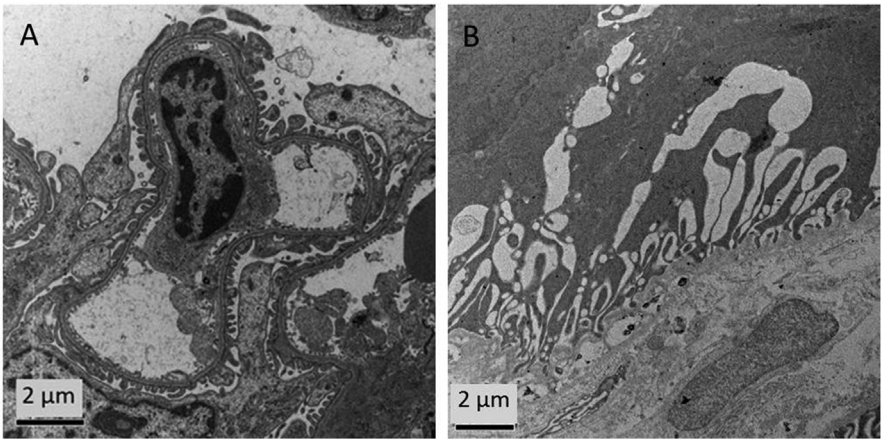

Fig. 8. TEM ultrastructural analysis of kidneys. TEM images of glomerular area of kidneys at (A) 10 minutes and (B) 1 month post PVA MBs injection.

Also for lungs the slight thickening of the alveolar septum, observed after 10 minutes post-injection (Fig. 9A), was fully recovered after one month (Fig. 9B).

The bioelimination ability of the liver after one month post-injection was tested. To this aim, 10 slices of the liver were analysed and the results at 10 minutes post-injection were compared to samples collected after 1 month. TEM micrographs of samples collected 10 minutes post-MB injection clearly showed the presence in the liver of structures (Fig. 10A) compatible with MBs in terms of shape and size [44] To discriminate the MBs from the lipid droplets often present in the liver and having similar size to MBs, EDX analysis was performed. Osmium tetroxide used in the tissue post-fixation (see Material andMethods section) stained specifically fat deposits. The absence of osmium (Os) in the round-shaped structures in the liver confirms the identification of PVA MBs. Moreover, TEM analysis of single-cell allows to identify PVA MBs as localised inside Kupffer cells macrophages (Fig. 10A).

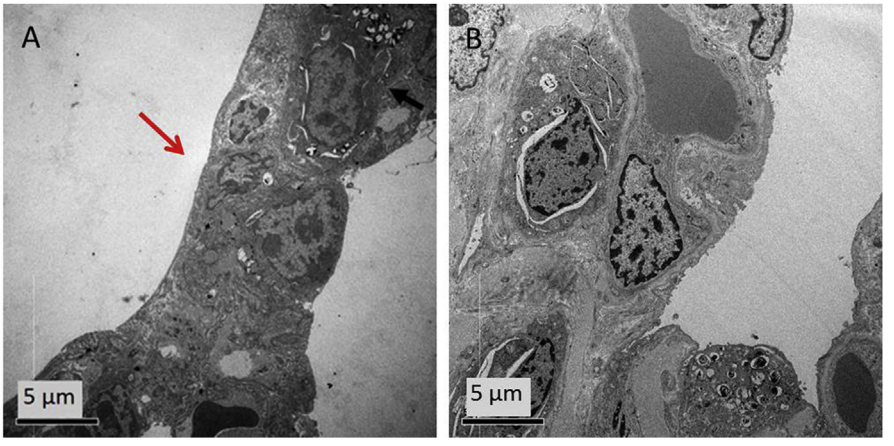

Fig. 9. TEM ultrastructural analysis of lungs. TEM images of pneumocytes at (A) 10 minutes and (B) 1 month post PVA MBs injection. The arrow points out the lung alveoli thickening.

https://doi.org/10.1016/j.heliyon.2018.e00770

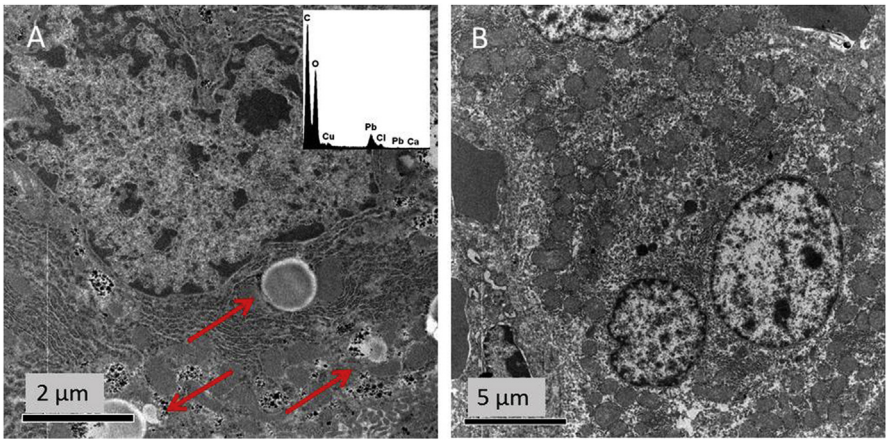

Fig. 10. TEM ultrastructural analysis of liver. TEM images of hepatocytes from liver after (A) 10 minutes and (B) 1 month post PVA MBs injection. Arrows indicate MBs. Elemental analysis of the MBs is shown in the insert.

After one month from the injection (Fig. 10B), MBs were absent in the liver: such finding can be directly caused by the occurrence of an elimination mechanism of PVA MBs. This behaviour is supported by a study on PVA MBs where macrophage phagocytosis is reported as the main mechanism responsible for their elimination [44].

4. Discussion

PVA MBs are IV injectable polymeric UCAs. As for all exogenous particles [45], once exposed to human plasma PVA MBs are covered by an external coating layer of protein usually termed "protein corona". These proteins including serum albumin, serotransferrins and a type of lipoproteins called dysopsonins, are found in the blood and favourably influence the MB biocompatibility. Other binding proteins of PVA MBs include opsonins, immunoglobulin G and complement C3 [46]. They promote events of phagocytosis that participate in the clearance of the exogenous substance from the bloodstream by the monocyte phagocytic system (MPS). However, it is important that the process of clearance is not too rapid so as to prevent UCAs from exerting their function.

The present work aims to determine the biological behaviour of PVA-based MBs once injected into the body. The well-known biocompatibility and "bioinertness" features of PVA have already permitted the use of this polymer for several applications in food and biomedical fields [47]. However, a construct based on a biocompatible material does not necessarily behave as biocompatible. Many issues must be considered such as size, shape and biointerface as well as chemical and physical modifications occurring during the fabrication of the construct.

https://doi.org/10.1016/j.heliyon.2018.e00770

The absence of PVA MBs cytotoxicity *in vitro* was previously assessed [35, 36]. This is the first study examining their *in vivo* biological distribution and bioelimination pathways. It should be pointed out that in a previous study on the MB biodistribution a phagocytic process sustained almost exclusively by the macrophages from lung and liver was highlighted by Barrefelt *et al* [48]. However, the surface and biointerface of such MBs were deeply different from the ones studied here, where the PVA shell is directly involved in all biointerface processes. As far as the MBs investigated in that study are concerned, the PVA surface was buried by a layer-by-layer process with the outermost layer composed of the negatively-charged sodium poly (styrene sulphonate) (PSS). On the contrary, the surface of the PVA MBs described in this work is neutral and the PVA is the unique material exposed to metabolites and tissues. It is well-known that the surface charge of the particle is one of the most important properties influencing both protein corona effect [49] and cell uptake by macrophages [50].

Moreover, it has been reported that the layer-by-layer MBs cause renal degeneration 4 hours after injection in mice [48] while the PVA MBs injected mice reported here were in good condition even after one month post-treatment.

The high tolerability of MBs was confirmed by the good general condition and by the absence of alterations in clinical parameters in injected mice. The IV administered MBs accumulated mostly in the liver and much less in the spleen, where the fluorescence signal decreased during the first 7 days of observation. Limited ultrastructural alterations, if any, were monitored in the kidneys, lungs, and liver 10 minutes post-injection, but they fully recovered after 1 month. The MBs were visualised in the hepatic phagocytic cells of the liver, i.e. the Kupffer cells after 10 minutes, nevertheless the clearance was not too fast since after 100 minutes from injection PVA MBs signal was present in most of the organs analysed. Due to their micron-size, MBs are not able to overcome the lining of the endothelium but they can be accessible to Kupffer cells since they are directly exposed to the bloodstream. The ability of phagocytic cells to engulf MBs has been assessed and confirmed both *in vitro* and *in vivo*. The hypothesised mechanism of PVA MBs bioelimination is ascribable to macrophages that have a known ability to produce reactive oxygen species that could lead to the oxidation and degradation of PVA polymer [51] and of the crosslinking points connecting the PVA chains in the network of the MBs shell. Alternatively MBs could be directly eliminated without degradation by the liver [17].

5. Conclusions

This work integrates the known physical and chemical properties of the PVA MBs with the first *in vivo* results on biodistribution/bioelimination of UCAs in mice. The

https://doi.org/10.1016/j.heliyon.2018.e00770

feasibility of the use of the MBs based on the PVA synthetic polymer in small animals was demonstrated by following the fate of the administered sample in a time window starting from minutes to weeks. The study confirms the absence of cytotoxic effects, also in the presence of the NIR dye, by qualitative observations of mice behaviour and image-based *in vivo* biodistribution as well as by quantitative measurements of animal weights, haematological and biochemical parameters and *ex vivo* analysis of organs.

These results, combined with the central role of macrophages in the elimination ability of MBs from the liver (identified as the main organ of accumulation) bring the PVA polymer shelled MBs a step further towards the *in vivo* application of PVA MBs in the next generation UCAs panorama.

Declarations

Author contribution statement

Barbara Cerroni: Conceived and designed the experiments; Performed the experiments; Analyzed and interpreted the data; Wrote the paper.

Rosella Cicconi, Letizia Oddo, Manuel Scimeca: Conceived and designed the experiments; Performed the experiments; Analyzed and interpreted the data.

Rita Bonfiglio, Roberta Bernardini, Graziana Palmieri, Fabio Domenici: Performed the experiments.

Elena Bonanno, Maurizio Mattei: Conceived and designed the experiments; Contributed reagents, materials, analysis tools or data.

Gaio Paradossi: Conceived and designed the experiments; Analyzed and interpreted the data; Contributed reagents, materials, analysis tools or data; Wrote the paper.

Funding statement

This work was partially funded by the EU Seventh Framework Programme FP7/2007-2013 “TheraGlio” (602923).

Competing interest statement

The authors declare no conflict of interest.

Additional information

No additional information is available for this paper.

https://doi.org/10.1016/j.heliyon.2018.e00770

List of acronyms

ALT	Alanine aminotransferase
AST	Aspartate aminotransferase
BUN	Blood urea nitrogen
CLSM	Confocal laser scanning microscopy
CRE	Creatinine
DMEM	Dulbecco's modified eagle medium
DyL	DyLight755
DyL-MBs	DyLight755-labelled PVA MBs
EDX	Energy dispersive x-ray
GRAN	Granulocytes
HCT	Haematocrit
HGB	Haemoglobin
IV	Intravenously
LYMF	Lymphocytes
MB	Microbubble
MCH	Mean corpuscular haemoglobin
MCHC	Mean corpuscular haemoglobin concentration
MCV	Mean corpuscular volume
MID	Mid-range cells
MPS	Monocyte phagocytic system
MPV	Mean platelet volume
MRI	Magnetic Resonance Imaging
NHS	N-hydroxysuccinimide
NIR	Near infrared
Os	Osmium
PCL	Polycaprolactone
PLA	Poly(DL-lactide)
PLGA	Poly(lactide-co-glycolide)
PLT	Platelet
PSS	Poly (styrene sulphonate)
PVA	Poly(vinyl alcohol)
RBC	Red blood cells
RDW	Red cell distribution width
ROI	Regions of interest
SEM	Scanning electron microscopy
SEM	Standard error of the mean
SST	Serum Separator Tube
TEM	Transmission electron microscopy
UCA	Ultrasound contrast agent
US	Ultrasound
WBC	White blood cells

https://doi.org/10.1016/j.heliyon.2018.e00770

References

[1] J.R. Lindner, Microbubbles in medical imaging: current applications and future directions, Nat. Rev. Drug Discov. 3 (6) (2004) nrd1417.

[2] K. Ferrara, R. Pollard, M. Borden, Ultrasound microbubble contrast agents: fundamentals and application to gene and drug delivery, Annu. Rev. Biomed. Eng. 9 (1) (2007) 415–447.

[3] S. Capece, F. Domenici, F. Brasili, L. Oddo, B. Cerroni, A. Bedini, F. Bordi, E. Chiessi, G. Paradossi, Complex interfaces in "Phase-change" contrast agents, Phys. Chem. Chem. Phys. 18 (12) (2016) 8378–8388.

[4] F. Calliada, R. Campani, O. Bottinelli, A. Bozzini, M.G. Sommaruga, Ultrasound contrast agents, Eur. J. Radiol. 27 (1998) S157–S160.

[5] A. Raisinghani, A.N. DeMaria, Physical principles of microbubble ultrasound contrast agents, Am. J. Cardiol. 90 (10A) (2002) 3J–7J.

[6] D. Grishenkov, C. Pecorari, T.B. Brismar, G. Paradossi, Characterization of acoustic properties of PVA-shelled ultrasound contrast agents: linear properties (Part I), Ultrasound Med. Biol. 35 (7) (2009) 1127–1138.

[7] D. Grishenkov, L. Kari, L.-K. Brodin, T.B. Brismar, G. Paradossi, In vitro contrast-enhanced ultrasound measurements of capillary microcirculation: comparison between polymer- and phospholipid-shelled microbubbles, Ultrasonics 51 (1) (2011) 40–48.

[8] M. Poehlmann, D. Grishenkov, S.V.V.N. Kothapalli, J. Härmark, H. Hebert, A. Philipp, R. Hoeller, M. Seuss, C. Kuttner, S. Margheritelli, G. Paradossi, A. Fery, On the interplay of shell structure with low- and high-frequency mechanics of multifunctional magnetic microbubbles, Soft Matter 10 (1) (2014) 214–226.

[9] F. Cavalieri, A. El Hamassi, E. Chiessi, G. Paradossi, Stable polymeric microballoons as multifunctional device for biomedical uses: synthesis and characterization, Langmuir ACS J. Surf. Colloids 21 (19) (2005) 8758–8764.

[10] M. Schneider, Characteristics of SonoVue™, Echocardiography 16 (1999) 743–746.

[11] S. Zhao, D.E. Kruse, K.W. Ferrara, P.A. Dayton, Selective imaging of adherent targeted ultrasound contrast agents, Phys. Med. Biol. 52 (8) (2007) 2055–2072.

[12] N.G. Fisher, J.P. Christiansen, A. Klibanov, R.P. Taylor, S. Kaul, J.R. Lindner, Influence of microbubble surface charge on capillary transit

 https://doi.org/10.1016/j.heliyon.2018.e00770

and myocardial contrast enhancement, J. Am. Coll. Cardiol. 40 (4) (2002) 811–819.

[13] J.K. Willmann, Z. Cheng, C. Davis, A.M. Lutz, M.L. Schipper, C.H. Nielsen, S.S. Gambhir, Targeted microbubbles for imaging tumor angiogenesis: assessment of whole-body biodistribution with dynamic micro-PET in mice, Radiology 249 (1) (2008) 212–219.

[14] Y. Watanabe, N. Hamada, M. Morita, Y. Tsujisaka, Purification and properties of a polyvinyl alcohol-degrading enzyme produced by a strain of pseudomonas, Arch. Biochem. Biophys. 174 (2) (1976) 575–581.

[15] E. Chiellini, A. Corti, S. D'Antone, R. Solaro, Biodegradation of poly (vinyl alcohol) based materials, Prog. Polym. Sci. 28 (6) (2003) 963–1014.

[16] M. Ullah, C. Weng, H. Li, S. Sun, H. Zhang, A. Song, H. Zhu, Degradation of polyvinyl alcohol by a novel bacterial strain Stenotrophomonas sp. SA21, Environ. Technol. 0 (0) (2017) 1–6.

[17] Y. Kaneo, S. Hashihama, A. Kakinoki, T. Tanaka, T. Nakano, Y. Ikeda, Pharmacokinetics and biodisposition of poly(vinyl alcohol) in rats and mice, Drug Metab. Pharmacokinet. 20 (6) (2005) 435–442.

[18] B. Cerroni, E. Chiessi, S. Margheritelli, L. Oddo, G. Paradossi, Polymer shelled microparticles for a targeted doxorubicin delivery in cancer therapy, Biomacromolecules 12 (3) (2011) 593–601.

[19] A. Galbiati, B. M. della Rocca, C. Tabolacci, S. Beninati, A. Desideri, G. Paradossi, PVA engineered microcapsules for targeted delivery of camptothecin to HeLa cells, Mater. Sci. Eng. C 31 (8) (2011) 1653–1659.

[20] A. Galbiati, C. Tabolacci, B. Morozzo Della Rocca, P. Mattioli, S. Beninati, G. Paradossi, A. Desideri, Targeting tumor cells through chitosan-folate modified microcapsules loaded with camptothecin, Bioconjug. Chem. 22 (6) (2011) 1066–1072.

[21] R. Villa, B. Cerroni, L. Viganò, S. Margheritelli, G. Abolafio, L. Oddo, G. Paradossi, N. Zaffaroni, Targeted doxorubicin delivery by chitosan-galactosylated modified polymer microbubbles to hepatocarcinoma cells, Colloids Surf. B Biointerfaces 110 (2013) 434–442.

[22] T.B. Brismar, D. Grishenkov, B. Gustafsson, J. Härmark, Å. Barrefelt, S.V.V.N. Kothapalli, S. Margheritelli, L. Oddo, K. Caidahl, H. Hebert, G. Paradossi, Magnetite nanoparticles can be coupled to microbubbles to support multimodal imaging, Biomacromolecules 13 (5) (2012) 1390–1399.

https://doi.org/10.1016/j.heliyon.2018.e00770

[23] G.D. Luker, K.E. Luker, Optical imaging: current applications and future directions, J. Nucl. Med. 49 (1) (2008) 1−4.

[24] V. Pansare, S. Hejazi, W. Faenza, R.K. Prud'homme, Review of long-wavelength optical and NIR imaging materials: contrast agents, fluorophores and multifunctional nano carriers, Chem. Mater. Publ. Am. Chem. Soc. 24 (5) (2012) 812−827.

[25] L. Oddo, B. Cerroni, F. Domenici, A. Bedini, F. Bordi, E. Chiessi, S. Gerbes, G. Paradossi, Next generation ultrasound platforms for theranostics, J. Colloid Interface Sci. 491 (2017) 151−160.

[26] M.I. Baker, S.P. Walsh, Z. Schwartz, B.D. Boyan, A review of polyvinyl alcohol and its uses in cartilage and orthopedic applications, J. Biomed. Mater. Res. B Appl. Biomater. 100 (5) (2012) 1451−1457.

[27] J.K. Li, N. Wang, X.S. Wu, Poly(vinyl alcohol) nanoparticles prepared by freezing-thawing process for protein/peptide drug delivery, J. Contr. Release Off. J. Contr. Release Soc. 56 (1−3) (1998) 117−126.

[28] F. Yoshii, Y. Zhanshan, K. Isobe, K. Shinozaki, K. Makuuchi, Electron beam crosslinked PEO and PEO/PVA hydrogels for wound dressing, Radiat. Phys. Chem. 55 (2) (1999) 133−138.

[29] M. Wang, Y. Li, J. Wu, F. Xu, Y. Zuo, J.A. Jansen, In vitro and in vivo study to the biocompatibility and biodegradation of hydroxyapatite/poly(vinyl alcohol)/gelatin composite, J. Biomed. Mater. Res. A 85 (2) (2008) 418−426.

[30] S. Kayal, R.V. Ramanujan, Doxorubicin loaded PVA coated iron oxide nanoparticles for targeted drug delivery, Mater. Sci. Eng. C 30 (3) (2010) 484−490.

[31] S.V. Ghugare, E. Chiessi, R. Fink, Y. Gerelli, A. Scotti, A. Deriu, G. Carrot, G. Paradossi, Structural investigation on thermoresponsive PVA/poly(methacrylate-Co-N-isopropylacrylamide) microgels across the volume phase transition, Macromolecules 44 (11) (2011) 4470−4478.

[32] A.B. Salunkhe, V.M. Khot, N.D. Thorat, M.R. Phadatare, C.I. Sathish, D.S. Dhawale, S.H. Pawar, Polyvinyl alcohol functionalized cobalt ferrite nanoparticles for biomedical applications, Appl. Surf. Sci. 264 (2013) 598−604.

[33] R. Dinarvand, N. Sepehri, S. Manoochehri, H. Rouhani, F. Atyabi, Polylactide-co-glycolide nanoparticles for controlled delivery of anticancer agents, Int. J. Nanomed. 6 (2011) 877−895.

https://doi.org/10.1016/j.heliyon.2018.e00770

[34] S. Grund, M. Bauer, D. Fischer, Polymers in drug delivery—state of the art and future trends, Adv. Eng. Mater. 13 (3) (2011) B61−B87.

[35] F. Cavalieri, A.E. Hamassi, E. Chiessi, G. Paradossi, R. Villa, N. Zaffaroni, Ligands tethering to biocompatible ultrasound active polymeric microbubbles surface, Macromol. Symp. 234 (1) (2006) 94−101.

[36] P. Mozetic, M. Tortora, B. Cerroni, G. Paradossi, Polymer based biointerfaces: a case study on devices for theranostics and tissue engineering, in: Ultrasound Contrast Agents, Springer, Milano, 2010, pp. 67−77.

[37] A. Carpentieri, E. Cozzoli, M. Scimeca, E. Bonanno, A.M. Sardanelli, A. Gambacurta, Differentiation of human neuroblastoma cells toward the osteogenic lineage by MTOR inhibitor, Cell Death Dis. 7 (2016) e2202.

[38] M. Dykstra, Biological Electron Microscopy: Theory, Techniques and Troubleshooting, Plenum Press, New York, 1992.

[39] E.S. Reynolds, The use of lead citrate at high PH as an electron-opaque stain in electron microscopy, J. Cell Biol. 17 (1963) 208−212.

[40] M. Scimeca, A. Orlandi, I. Terrenato, S. Bischetti, E. Bonanno, Assessment of metal contaminants in non-small cell lung cancer by EDX microanalysis, Eur. J. Histochem. 58 (3) (2014).

[41] M. Scimeca, S. Bischetti, H.K. Lamsira, R. Bonfiglio, E. Bonanno, Energy Dispersive X-ray (EDX) microanalysis: A powerful tool in biomedical research and diagnosis, Eur. J. Histochem. 62 (1) (2018) 2841.

[42] S. Gioux, H.S. Choi, J.V. Frangioni, Image-guided surgery using invisible near-infrared light: fundamentals of clinical translation, Mol. Imaging 9 (5) (2010), 7290.2010.00034.

[43] M. Ahmed, B. Cerroni, A. Razuvaev, J. Härmark, G. Paradossi, K. Caidahl, B. Gustafsson, Cellular uptake of plain and SPION-modified microbubbles for potential use in molecular imaging, Cell. Mol. Bioeng. 10 (6) (2017) 537−548.

[44] J. Härmark, M.K. Larsson, A. Razuvajev, P.J.B. Koeck, G. Paradossi, L.-Å. Brodin, K. Caidahl, H. Hebert, A. Bjällmark, Investigation of the elimination process of a multimodal polymer-shelled contrast agent in rats using ultrasound and transmission electron microscopy, Biomed. Spectrosc. Imaging 4 (1) (2015) 81−93.

[45] C. Sacchetti, K. Motamedchaboki, A. Magrini, G. Palmieri, M. Mattei, S. Bernardini, N. Rosato, N. Bottini, M. Bottini, Surface polyethylene glycol conformation influences the protein corona of polyethylene glycol-modified

https://doi.org/10.1016/j.heliyon.2018.e00770

single-walled carbon nanotubes: potential implications on biological performance, ACS Nano 7 (3) (2013) 1974−1989.

[46] S. Wan, G. Egri, L. Oddo, B. Cerroni, L. Dähne, G. Paradossi, A. Salvati, I. Lynch, K.A. Dawson, M.P. Monopoli, Biological in situ characterization of polymeric microbubble contrast agents, Int. J. Biochem. Cell Biol. 75 (2016) 232−243.

[47] C.A. Finch, Polyvinyl alcohol; properties and applications, Wiley, London, New York, 1973.

[48] Å. Barrefelt, Y. Zhao, M.K. Larsson, G. Egri, R.V. Kuiper, J. Hamm, M. Saghafian, K. Caidahl, T.B. Brismar, P. Aspelin, R. Heuchel, M. Muhammed, L. Dähne, M. Hassan, Fluorescence labeled microbubbles for multimodal imaging, Biochem. Biophys. Res. Commun. 464 (3) (2015) 737−742.

[49] P. Aggarwal, J.B. Hall, C.B. McLeland, M.A. Dobrovolskaia, S.E. McNeil, Nanoparticle interaction with plasma proteins as it relates to particle biodistribution, biocompatibility and therapeutic efficacy, Adv. Drug Deliv. Rev. 61 (6) (2009) 428−437.

[50] F. Ahsan, I.P. Rivas, M.A. Khan, A.I. Torres Suarez, Targeting to macrophages: role of physicochemical properties of particulate carriers–liposomes and microspheres–on the phagocytosis by macrophages, J. Contr. Release Off. J. Contr. Release Soc. 79 (1−3) (2002) 29−40.

[51] K. Sutherland, J.R. Mahoney, A.J. Coury, J.W. Eaton, Degradation of biomaterials by phagocyte-derived oxidants, J. Clin. Invest. 92 (5) (1993) 2360−2367.

https://doi.org/10.1016/j.heliyon.2018.e00770